Paper 93
Optimisation of Aspects of Helicopter Rotor Blades and Fuselage

C.S.Johnson[†] and G.N.Barakos[*]
School of Engineering, University of Liverpool, L69 3GH, UK
www.liv.ac.uk/engdept

This work presents a method for the optimisation of aspects of rotor blades in hover and forward flight and for the parameterisation and optimisation of idealised helicopter fuselages. The proposed technique employs CFD in conjunction with artificial neural networks (ANNs) and genetic algorithms (GAs). The developed method was used to optimise the anhedral and sweep of the UH60-A rotor blade in forward flight. The resulting twist was then optimised for in hover. A parameterisation method was defined, a specific objective function was created using the initial CFD data and the meta-model was used for evaluating the objective function during the optimisation. For fuselage optimisation, the parameterisation method was based on the super-ellipsoid method used for the ROBIN body. The obtained results suggest optima in agreement with engineering intuition but provide precise information about the shape of the final geometries and their performance. The results were checked using different optimisation methods and meta-models and were not sensitive to the employed techniques with substantial overlap between the outputs of the selected methods. The main CPU cost was associated with populating the CFD database necessary for the meta-model.

Nomenclature

Latin

AR	Aspect ratio
C	Generic aerodynamic coefficient
E	Error
h	Hidden layer
k	Reduced frequency, $\frac{c\omega}{U_\infty}$
k	Turbulent kinetic energy in $k-\omega$ model
M	Mach number
N_{blade}	Number of blades
R	Length of blade, radius of rotor
Re	Reynolds number
U	Velocity component in x-direction

Greek

Δ	difference between max and min
η	Learning rate of ANN
μ	Advance ratio
ω	Angular velocity
Ψ	Azimuth angle
∇	Gradient
Ψ	Azimuth angle
∇	Gradient

Acronyms

ANN	Artificial Neural Networks
CFD	Computational Fluid Dynamics
GA	Genetic Algorithm
HMB	Helicopter Multiblock Solver
JMRTS	JAXA Multi-purpose Rotor Testing System
LHS	Latin Hypercube Sampling
NACA	National Advisory Committee for Aeronautics
OFV	Optimisation Function Value
RANS	Reynolds Averaged Navier-Stokes

Subscripts and Superscripts

adv	Advancing side
avg	Average
$\overline{C}$	Average value of C
disk	Coefficient over the full disk
max	Maximum
min	Minimum
p	Pressure
pitch	Pitching moment coefficient
Q	Torque
ref	Reference
ret	Retreating side (of rotor disk)
T	Thrust
vib	Vibratory
∞	Freestream value

1 Introduction

Rotor blade optimisation is becoming an increasingly important part of the design process as engineers push further and further the boundaries of rotorcraft efficiency and performance. From the outset, the development of optimisation techniques has progressed quite quickly in the structural aspect of rotor design[1] for various objectives such as vibration reduction[2,3]. This was not the case on the

[†]PhD Candidate, C.S.Johnson@liv.ac.uk
[*]Professor, G.N.Barakos@liv.ac.uk.

aerodynamic front due to the lack of efficient and accurate modelling techniques[4,5] although there has been significant improvement[5]. Nevertheless, several authors[4,6-12] have attempted to devise a variety of successful optimisation techniques. However, each method is typically limited either by the efficiency of the method or the accuracy of the results. The reason for this is that high-fidelity CFD simulations are necessary to accurately capture the effects of design changes, especially for rotor aerodynamics but a number of these CFD solutions are required for the process and each calculation can take a long time at a significant computational cost. The variables that have a relatively large effect on the performance of rotor blades are twist, tip sweep, anhedral, blade taper and the selection of aerofoils[5,14-17]. These are typically optimised for hover and forward flight conditions. Initially, gradient-based methods were developed such as CONMIN[18], as they were faster than non-gradient based methods. CONMIN was and is still one of the most frequently used gradient-based methods. Le Pape and Beaumier[7] used it to optimise rotor Figure of Merit (FM) in hover, and Walsh[6] used it to optimise rotors in hover with added constraints needed to maintain forward flight performance. However, in both of these cases, the optimum was highly dependent on the starting point in the design space, and improved blade performance was obtained mainly due to the very poor initial design. This is typical of gradient-based optimisation in a highly uneven design space. Further, the employed aerodynamics was based on blade element analysis methods.

To overcome the problem of the gradient based methods getting trapped in local optima, Schwabacher, Ellman and Hirsh[19] used gradient-based methods to optimise aircraft wings and yacht hulls shapes. They also employed a learning algorithm to determine where the best initial design point should be. Chen and Lee[20] also tried to improve gradient based methods by using a gradient-forecasting search method (GFSM) to dynamically adjust the prediction steps to overcome local optima. Gradient-based methods were also used by Mohammadi and Pironneau (2004)[21] who performed multi-criteria shape optimisation of a business jet by applying second-order Newton and quasi-Newton gradient-based methods. They concluded that an optimal method would perhaps be a hybrid method including both gradient and non-gradient based methods.

Non-gradient based methods have recently become more popular, primarily for steady state aerodynamic optimisation, as they require less computational time. Watanabe, Matsushima and Nakahashi[22], for example, used Euler simulations with a genetic algorithm (GA) to optimise a passenger plane wing for shock wave alleviation. Another area that has benefited from non-gradient based optimisation is engine turbine and compressor blade design[23,24]. Mengistu and Ghaly[25] successfully used evolutionary methods to optimise turbo-machinery blades and were successful in their task. However, even for their case, the blades were optimised for a single design point.

To some extent, non-gradient methods have also been used for rotor optimisation but have not been fully explored because of the high computational and time cost that limits the practical use of it. Le Pape[26] extended his work[7] to include forward flight optimisation and in doing so, developed a hybrid method capable of using gradient based (CONMIN) *and* non-gradient based techniques (Genetic Algorithms). This new approach allowed for the optimisation of anhedral, sweep, twist, chord and aerofoil distribution using aerofoil data from an existing database. The method allowed parts of the blade, or the full blade to be optimised. Hover performance could be constrained while forward flight is optimised and vice versa. However, because of the use of lower fidelity aerodynamic methods especially for forward flight, like *HOST* (where for this case the aerodynamics were modelled using lifting-line theory[26]), to reduce CPU cost and time to obtain the initial data, the results were not very accurate for complex blades and shapes. However, by modifying the objective function, the optimiser was forced to work within the limitations of the models and hence the obtained results were still valid.

In the optimisation technique used by Imiela[8], hover and forward flight were both considered and optimised successfully for aerodynamic performance while constraining structural loads within given boundaries. However, due to the high computational cost of the objective function evaluations for rotors in forward flight, only one parameter was optimised and this was still at a considerable computation cost although not specified explicitly. Even in the hover case, optimising seven parameters required a considerable amount of time. The high cost of CFD computations is an issue mentioned by several authors; one of the ways of overcoming this difficulty is to use a model of the CFD solution, a meta-model or surrogate model, as predicted by Ganguli[5].

Allen, Rendall and Morris[12] used an interpolation method in their optimisation. In their work, they started with aerofoils and fixed wings and eventually attempted to optimise rotors in hover. Glaz, Friedmann and Liu[9,10] successfully used non-

gradient surrogate-based optimisation for vibration reduction starting with a baseline BO-105 rotor. Tatossian, Nadarajah and Castonguay[11] took a different approach to shape optimisation of hovering rotors, improving the adverse transonic flow effects at tip Mach numbers of 0.85 and above. They used a discrete adjoint-based aerodynamic optimisation algorithm based on a non-linear frequency domain approach and employed control theory to modify the shape interactively. More recently, Chae, Yee, Jeong and Obayashi[13] optimised rotor blade shapes to reduce high speed forward flight noise and induced power, whilst constraining the autorotation capability among other constraints. They used Genetic Algorithms (GAs) with a Kriging meta-model to find the best design compromise between the performance and noise reduction objectives. In the work of Celi[4], GAs appear to have potential for the future though gradient-based methods are of widespread use. In recent years, increased capacity of computers and advances in algorithms allowed for GAs to be used for practical calculations.[8,42]

Fuselage drag is a high contributor to the overall drag of a helicopter because of its bluff body in addition to the other non-streamlined components such as non-retractable landing gear, weapons etc. In addition, helicopters tend to yaw and fly at high angles of attack which makes it difficult to obtain a streamlined fuselage at all conditions. Hence, the objective for fuselage optimisation is to reduce the overall drag in forward flight, within practical constraints such as volume of the body or specific geometric features that must be preserved.

The work described here aims to demonstrate a framework allowing different aspects of rotors and fuselages to be optimised given an existing design as a starting point. For real helicopters, the initial designs would already be near optimum and the aim is to capture the aerodynamic effects of any design changes and adjust these design variables to find an optimum value for them. The novelty of this method is the use of a meta-model in conjunction with high-fidelity CFD data so that high-resolution performance improvements can be captured efficiently. A non-gradient based method is used coupled with a meta-model to improve its efficiency. The method has been used previously for transonic aerofoil optimisation, wing planform for elliptic load distribution, rotor twist in hover and rotor sections of a forward flying rotor, inboard and outboard[42]. In this paper, the optimisation of the UH60-A rotor anhedral and sweep in forward flight and its twist in hover are explained in detail. This case is more interesting as the effects of combined anhedral and sweep on a rotor blade are not fully explored. The method is also expected to be applied to the optimisation of BERP-like blades. Also in this paper, is the optimisation of the parameterised JMRTS (JAXA Multi-purpose Rotor Testing System) fuselage developed by JAXA[45]. With these examples, it is shown that an objective function can be created that captures the optimum design and that using meta-models, specifically artificial neural networks (ANNs), the trend in this objective function can be predicted. The optimum is found and analysed, a-posteriori, using a high-fidelity CFD solver. The next section of this paper presents the details of the method, and this is followed by a discussion of the obtained results and conclusions.

2 Method

Figure 1 is a summary of the optimisation procedure. The optimisation procedure relies on an initial database of designs and their performance. CFD is used to obtain this data using a high-fidelity solver to capture the performance changes caused by changes in the design variables. The database is then expanded using an interpolation method by the meta-model. The use of the meta-model increases the efficiency of the optimisation process without limiting the options available to the optimiser. A number of meta-models were employed and artificial neural networks (ANNs) and Kriging were found to be the most viable in terms of accuracy. It was found that the former was more accurate and robust for the cases presented. The meta-model is then coupled with a genetic algorithm (GA) for the optimisation. The GA works similarly to the natural world's evolutionary system of 'survival-of-the-fittest'. Here, however, the population is the database of individual design points, each with a 'fitness' value reliant on the predictions of the meta-model and evaluated using an objective function. The GA would allow new designs to be created and would eventually create a population that is highly optimised for the specified objectives. The objective function is a key part of the process as it must capture the objectives using the performance parameters available. The parameterisation method is also important as it must represent the design accurately with as few parameters as possible for the full process to work efficiently. The development of the method is documented in Johnson and Barakos[41–43]. To demonstrate the capabilities of this method, the optimisation of the rotor tip of the UH60-A rotor blade in forward flight is used. In addition, the method is applied to the JMRTS fuselage developed by JAXA.

2.1 CFD solver and Grid Generation

The Helicopter Multiblock Solver (HMB) was used to obtain high fidelity CFD data. This code has been validated against a wide range of aerodynamic and aeroelastic cases that include rotors in hover and forward flight. For these cases HMB solves the RANS equations using a cell-centred finite volume approach on structured multiblock grids. Temporal integration is done using an implicit dual-time stepping method. It is able to use a number of turbulence models and the $\kappa - \omega$[31] model was used for all cases presented in this paper. The solver is documented in many references[28,32,37,41] and the details of the CFD method are not given here.

For the forward flight case, a grid was generated for a quarter of the flow domain, and copied around the azimuth four times to obtain the full domain containing approximately nine million cells. For the hover case, only a quarter segment was used with periodic boundary conditions as the solution is assumed to be the same for each blade. In both cases, a spacing of 1×10^{-5} ($y^+ > 1$) chords was used perpendicular to the rotor surfaces. The blade mesh can be seen in Figure 3. The boundary conditions at the far field are set to free stream. The top farfield was set at 2R above the rotor plane, the bottom farfield at 4R below the rotor plane and the radial farfield at 4R from the hub centre, where R is the radius of the rotor.

For the fuselage, steady calculations were carried out on a circular grid that contained an O-grid which contained the fuselage. The grid size was approximately 3 million cells. Again, the spacing at the surface was approximately ($y^+ > 1$) chords.

2.2 Parameterisation

The parameterisation for the rotor anhedral, sweep and twist are simply the values of the angle that define them. However, for the fuselage, a more elaborate parameterisation technique is required. The method used is based on the super-ellipse equations used on the ROBIN body[44]. These equations are defined as follows:

$$\left(\frac{x+x_o}{A}\right)^n + \left(\frac{y+y_o}{B}\right)^m = C \qquad (1)$$

For this parameterisation, the longitudinal axis of the fuselage is always specified on the x-axis. The fuselage is then defined as a number of cross-sections along this axis (stations). Therefore, the varying co-ordinates of these stations are the y and z co-ordinates. The y and z coordinates at each station are defined by the centre of the station (Y_o, Z_o), its height and width (H, W) and the curvature of the section at its corners at the top and bottom (N, Nb). These six parameters are defined as a function of x. For generalisation, let the six parameter be called y for now. Then if Equation 1 is rearranged so that y is given in terms of x, it becomes:

$$y = B\left[C - \left(\frac{x+x_o}{A}\right)^n\right]^{1/m} - y_o \qquad (2)$$

To represent y in polar co-ordinate form, the following must be true,

$$y + y_o = rcos\phi \qquad (3)$$
$$x + x_o = rsin\phi \qquad (4)$$

where r is the radius of the polar circle. Substituting these into Equation 2,

$$(y+y_o)^m = B^m\left[C - \left(\frac{x+x_o}{A}\right)^n\right] \qquad (5)$$
$$(rcos\phi)^m = B^m\left[C - \left(\frac{rsin\phi}{A}\right)^n\right] \qquad (6)$$

which after some re-arrangement becomes,

$$r^m B^m cos^m\phi + r^n A^n sin^n\phi = A^n B^m C \qquad (7)$$

For this to be in polar co-ordinate form, m = n and C = 1. Therefore,

$$r^n\left(B^n cos^n\phi + A^n sin^n\phi\right) = A^n B^n \qquad (8)$$

Therefore,

$$r = \left[\frac{A^n B^n}{B^n cos^n\phi + A^n sin^n\phi}\right]^{1/n} \qquad (9)$$

where now, A = radius vertically = H/2, B is the radius horizontally = W/2 and n is the power of the ellipse which is N. Therefore r and the y and z coordinates are given by,

$$r = \left[\frac{\left(\frac{H}{2}\frac{W}{2}\right)^N}{\left(\frac{W}{2}cos\phi\right)^N + \left(\frac{H}{2}sin\phi\right)^N}\right]^{1/N} \qquad (10)$$
$$y = rsin\phi + y_o \qquad (11)$$
$$z = rcos\phi + z_o \qquad (12)$$

and the parameterisation coefficients are given as:

$$h, w, y_o, z_o, n, nb = C_7\left[C_1 + C_2\left(\frac{x+C_3}{C_4}\right)^{C_5}\right]^{1/C_8} + C_6 \qquad (13)$$

where C is a parameterisation coefficient. For the JAXA JMRTS fuselage, 10 segments were used with 6 variables (8 coefficients each) in each segment, to represent the shape. The comparison between the

recreated shape and the original shape can be seen in Figure 4 which also includes the experimental data of the fuselage. The separation at the back of the fuselage does not occur due to the lack of the hub on the fuselage, which was present in the experimental data. The pressure distribution at a number of stations along the longitudinal axis is also shown in Figure 5. The parameters are given in Table 1.

2.3 Meta-models

2.3.1 Artificial Neural Networks (ANN)

An ANN interpolates based on patterns obtained from a set of data. Figure 6 is a schematic of the structure of a multilayer feed-forward ANN. It consists of a number of neurons connected to every other neuron in the next layer, from input to output[37]. The layers between the input and output are known as hidden layers. Each neuron is associated with a weight and an activation function. The weight determines how much influence a neuron has on the output and the activation function keeps the values within bounds and gives the ANN the ability to be differentiable so that error corrections can be made using, for example, a gradient descent method.

There are two phases for ANNs viz. training and predicting. In the training phase, all the data is available to the ANN, that is, both input and output. The weights of the neurons are randomly chosen and the ANN makes a prediction. The error between this predicted output and the target output is then fed-back through the layers and the weights are adjusted accordingly. The full set of data, known as an epoch, is fed in repeatedly and the error back-propagated until the error converges to a pre-set value.

Once the ANN is trained, it can now be used to predict the output for any input within the limits trained with. This is the prediction phase of the ANN. For the ANNs used in the cases presented, the activation function used is a sigmoid function (Eqn 14) where u_j is the sum of the weighted inputs upto that hidden layer. Also all the values were first normalised to between 0 and 1 to maximise the use of the more linear part of the sigmoid curve as it improves the numerical accuracy. The predicted outputs are then de-normalised.

$$\sigma = 1/(1 + e^{-u_j}) \tag{14}$$

The optimum number of hidden layers depends on the complexity of the problem. In general, increasing the number of layers makes an ANN smarter and increasing the number of neurons per layer makes an ANN more accurate[37]. Typically, however, the number of hidden layers is kept to a maximum of two. To improve the speed of training the ANN, a learning rate and momentum is used that allows the ANN to skip a number of steps periodically before the weights are modified as a ratio of the last written weights. In this case, the learning rate is adaptive, in that it increases when the drop in error is large and decreases when the drop in error is small. This further improves the efficiency of training. During training, the inputs are also introduced in random order to prevent the ANN from 'memorising' and improve its prediction capabilities. The choice of parameters for the ANN were determined and validated using additional CFD data that was not included in the training data. It was found that in all cases 2 hidden layers with 15 neurons provided accurate predictions. Also, predicting each output separately prevented the ANN from overfitting the curves to the data and improved the speed of training. More details about the ANN tuning and performance can be found in Johnson and Barakos (2010)[41].

2.3.2 Kriging

The Kriging meta-model was also considered as an alternative to the ANN. This method uses sample data points to build a model that can be used to predict the output or performance of interpolated design points by fitting a low-order polynomial through the data points, but allowing the predictions along these polynomials to deviate based on a Gaussian distribution of all the existing points. This deviation allows the Kriging meta-model to fit the data with a smoother hyperplane as it does not have to strictly fall within a given tolerance of the points. The regression function used to fit the data defines the smoothness of the hyperplane too. The Gaussian distribution's characteristics are based on the correlation between the sample points i.e. on their proximity to each other. This allows the Kriging parameters to change with the prediction point giving it more flexibility. So, the output or performance, P is represented as:

$$P(x, y) = f(x, y) + Z(x, y) \tag{15}$$

where P(x) is the output or performance of the data, f(x) is the polynomial or regression function and Z(x) is the 'random process' that is based on the Gaussian distribution. For the polynomial fit, up to second order polynomials are common. In some cases, such as those presented in this paper, constant values, such as the mean value of all the data or linear polynomials are sufficient. The correlation between all the sample points with each other and between the required point and all the points is found as the Gaussian distribution of the distances between the points with a 'roughness' parameter, θ

for each design parameter[39] as shown in Equation 16. All the parameters and values are normalised and then de-normalised at the end so that the mean of Z(x,y) is 0. Also, the data is normalised in a scalar way over each parameters between 0 and 1.

$$\begin{aligned} Cov(i,j) &= exp\left(-\sum\left[\theta_x(x_i-x_j)^2+\theta_y(y_i-y_j)^2\right]\right) \\ &\text{or} \quad exp\left(-\sum\left[d^2\right]\right) \\ Cov(i,r) &= exp\left(-\sum\left[\theta_x(x_i-x_r)^2+\theta_y(y_i-y_r)^2\right]\right) \end{aligned} \tag{16}$$

where i and j are the sample points, r is the required point, x and y are the parameters, θ is the corresponding 'roughness' factor and d is the distance between the points.
The weight, λ can then be found as

$$\lambda = Cov(i,j)^{-1}Cov(i,r) \tag{17}$$

Then the prediction can be made as

$$\hat{P} = \lambda P(x) \tag{18}$$

The Kriging meta-model was implemented in a similar way to the MATLAB DACE toolbox,[40] however, a stand-alone implementation in FORTRAN was created, using *linpack*, a library of FORTRAN subroutines for matrix manipulation. The following subroutines were used: *sgedi, sgeco, sgefa, sscal, saxpy, isamax, sswap, sasum, sdot and schdc.* This allowed it to be used in conjunction with the optimisation algorithm. Similarly to the ANN case, the data is first normalised before the process is applied and then de-normalised.

2.4 Optimisation Method

For the optimisation, a non-gradient method in the form of a genetic algorithm (GA) was implemented and combined with the meta-models. Figure 7 shows the analogy and terminology used as applied to the optimisation of an aerofoil case: Selection, Crossover, Mutation, Competition, Survival. Two parents are first selected based on a roulette wheel technique. The roulette wheel is a file containing the full population of design points. However, each design point takes up as much space in the file as is proportional to its fitness or performance by duplication. A random selection is made from it, but since the wheel itself is biased towards fitter individuals the evolution leads to better designs being created. The proportionality function for space on the roulette wheel is user-defined from linear to exponential and is necessary for convergence and stability. This is because if the number of individuals in the database is very high, the percentage of space taken up by fitter individuals on the roulette wheel reduces and the selections become less biased and more random. Therefore a better fitness assignment rule would be an exponential one rather than a linear one for example. However, in this case a linear proportionality function sufficed.
Once the parents are selected, their 'genes' are swapped or crossed over. So in the illustration in Figure 7 either the thickness or camber is selected randomly and swapped between the two aerofoils.
For the mutation stage, the offspring parameters are converted to binaries of 10 bits of which a random bit is chosen and changed to either 1 or 0. Mutation is necessary since it has been found that after a number of generations, some characteristics of the genes get 'lost'[27]. Mutation allows for these characteristics to be re-introduced into the gene pool and it also increases diversity which allows the global optimum to be found.
The resulting offspring is then assessed by employing the trained ANNs and combining their output using the user-defined objective function. Originally, the attempt was to limit the data so that offspring that were outside the boundaries were excluded, but this reduced the diversity causing the GA to terminate pre-maturely before the global optimum was found. So instead, a penalty technique where instead of exclusion, a penalty value was added to the fitness of the offspring but it was allowed to be present in the new gene pool was used. This increased the efficiency and the ability of the GA to reach the global optimum.
After a number of such iterations, a pool of the offspring characteristics is created and a threshold value is set so that only the majority of the fitter individuals survive and pass on into the next generation pool. The fittest individuals are always carried through into the next generation. This is termed elitism. While the GA can converge without the help of elitism, the convergence takes longer and has a lower probability of being the global maximum since only mutation is capable of re-introducing new design characteristics or 'alleles' back into the pool and these may not be the best designs. Using elitism ensures that the best genes still exist in the gene pool (or 'live longer') and hence there is a higher probability of reaching the maximum value. Cloning is avoided as it can change the selection process unfairly.

The objective function for selection is a combination of the performance parameters weighted appropriately in order to capture the objective of the optimisation. The weights for the function are guided by the initial CFD data. Say for example, the optimisation was primarily for drag reduction but also to keep moments close to zero. For each design point a ratio can be found between drag and moment. Assume the average of all these ratios is 1:1.5 for drag as to moment. Then the limiting weight to weigh

drag more than moment in the objective function is 1.5/(1+1.5) = 0.6, i.e. on average, the weight of the drag must be ≥ 0.6. However, this should only be used as a guidance value, as individually, the deviation from this ratio can be large.
The objective function method differs from what is known as the Pareto method of optimisation. The Pareto method tries to find the best compromise in performance for the designs, i.e. an increase in one performance parameter results in a decrease in the other. Therefore it creates a boundary or front of design points. The objective function method however, tends to concentrate the optimum designs to a cluster in the design space as opposed to spreading the optimum design along a front i.e. it selects designs in a region of the Pareto front. The Pareto front method is found in a similar way to the objective function method, except the weights of the components are equal. Also, the elite members of the population are no longer the fittest individuals, but the ones that fulfil the Pareto conditions. In this work, both methods were used and the results show that the selected optima were also members of the Pareto front.

3 Results and Discussion

3.1 UH60-A Computations

For this case, the UH60-A rotor was used as a starting rotor. This rotor has an AR of 15.5. It has a tip sweep of 20^o and there is also a reversal of twist near the tip. Figure 8 shows the twist and aerofoil distribution for the UH60-A blade. Also, blade deformation was used with five harmonics to simulate the aeroelasticity of the blade as obtained from Datta and Chopra[33].
The rotor was run at a tip Mach number of 0.642, with $M_\infty = 0.236256$, resulting in $\mu = 0.368$. The Reynolds number for the forward rotor disk motion was 0.5×10^{-6}. The trim conditions were set with a collective of 11.6 degrees, a coning angle of 3.43 degrees, a single flap harmonic with -0.7 for the cos term and -1.0 for the sin term, a single pitch harmonic of -2.39 for the cos term and 8.63 for the sin term and no lag harmonics. The nominal blade twist is -9.76 degrees. For the scaled model with centre (0,0,0), the coordinates of the flap hinge are (1,0,0), for the lag hinge are (1.1,0,0) and for the pitch centre (1.5,0,0). The sideslip was set to -7.31.

The HMB RANS solver was used to obtain the original CFD data. The objective for forward flight was to optimise the UH60-A rotor anhedral and sweep to reduce the pitch loads, stall on the retreating side and shock effects on the advancing side whilst maintaining or improving the thrust, torque and vibratory loads. This objective can be captured with an objective function that includes the average and peak-to-peak pitching moments and constraints for the margin of change in thrust, torque and vibratory moments. The design points for the anhedral optimisation were obtained by translating the tip edge down and forming an arc between the end section of the blade where the sweep starts (approx r/R = 0.95) and the tip. The anhedral was then defined by the rotation angle of the arc. Figure 9 shows how the anhedral variation was incorporated into the blade design.

Four values of anhedral were used to obtain the CFD training data: 0, 5, 10 and 15 degrees and five values of sweep: 0, 10, 20, 30 and 40 degrees. The table also shows that the C_T for all the designs were within 3.6% of each other and this can be further reduced with re-trimming. For C_Q, the coefficients were within 4.8% of each other. Therefore the thrust and torque constraint was relaxed as long as the anhedral and sweep values were constrained within the boundaries of the database. That is, the points that violated these constraints were included in the next generation but were penalised first.
The effect of anhedral can be seen in the results for the M^2C_n and M^2C_m shown in Figures 10 which are for the extreme values of the database i.e. 0 and 15 degrees anhedral. Adding more anhedral loads the back of the disc more which distributes the disk loading more evenly. Sweep has the same effect as shown in Figure 11 for the 20 and 40 degree cases. The full and vibratory pitching moments for the blade from 0 to 360 degrees azimuth are shown in Figure 12 for varying sweep and anhedral. Adding more sweep decreases the peak-to-peak change in pitching moment and adding anhedral moves the average pitching moment closer to zero pitching moment. However, adding both of these increases the vibratory pitching moment. By vibratory, it is meant the oscillations in the moment variation after the mean moment is taken away. Also the effect of anhedral is more significant with more sweep. To capture the objectives, the average pitching moment ($\overline{C_m^{pitch}}$) and the overall peak-to-peak pitching moment ($\Delta C_m{}^{\text{pitch}}$) would make up the components of the objective and the vibratory pitching moment peak-to-peak ($\Delta C_m{}^{\text{vib-pitch}}$) value and torque coefficient would be constrained. In this work, $\Delta C_m{}^{\text{vib-pitch}}$ is defined as the total $C_m{}^{\text{pitch}}$ mean and 1 per rev. The parameterisation was simply the value of the anhedral and the sweep in degrees. The two components of the objective function are to be weighted equally. However, since on average, the

ratio of $\Delta C_m{}^{\text{pitch}}$ to $\overline{C_m^{pitch}}$ is 1.164:1, the weights of this function that would weight them equally were found to be:

$$\frac{1}{n}\sum_{i=0}^{n}\frac{\Delta C_m^{pitch}}{\overline{C_m^{pitch}}} = 1.164 \quad (19)$$

$$\Delta C_m^{pitch} : \overline{C_m^{pitch}} = 0.47 : 0.53 \quad (20)$$

So the overall objective function is:

$$\begin{aligned} OFV &= -0.47\Delta C_m^{pitch} - 0.53\overline{C_m^{pitch}} \\ &\quad +1, \text{if} \Delta C_m^{vib-pitch} \leq 5\% \\ &\quad \text{and scaled } C_Q \leq 1.0 \end{aligned} \quad (21)$$

$$\begin{aligned} \text{or, } OFV &= -0.47\Delta C_m^{pitch} - 0.53\overline{C_m^{pitch}} \\ &\quad +1 - 0.5(\Delta C_m^{vib-pitch} - \\ &\quad 1.05) - 0.5(C_Q - 1.02) \end{aligned} \quad (22)$$

All the performance values of the design points were scaled with a reference rotor, which was the original rotor in this case. These scaled values were used to train the ANN.
The GA was then used to find the optimum design using 500 iterations over five generations. $\Delta C_m{}^{\text{vib-pitch}}$ was constrained to be not more than 5% higher than that of the original blade and C_Q not more than 2%. The result are also shown in Figure 13(a). From the ANN predictions, the best performing designs are shown in Table 2 in scaled values. The average, peak-to-peak moments, and torque coefficient are reduced and there was a 5% increase in vibratory peak-to-peak moment. The optimum sweep and anhedral were found to be 17.1 degrees and 11 degrees respectively. The optima selected by the GA also lies on the Pareto front as shown in Figure 13(b). Again, it can be seen that the objective function method confines the optima to a region of the design space as opposed to a spread of the best compromise between the design points.

The hover analysis was then carried out. The twist of the forward flight optimised planform was optimised for in hover. The objective was to obtain a high Figure of Merit (FM) but to also maintain that FM for a range of thrust values. Therefore 2 performance parameters were used to capture this objective; maximum FM(FM_{max}) and the gradient of FM w.r.t. C_T (∇FM). In order to build this database, three twist parameters were selected and for each of them, the FM, C_T and C_Q were obtained for a range of three collective settings, resulting in a total of 9 HMB computations. ANNs were then used to predict the FM for a range of twist values and collective settings (Figure 14) and the predictions from these ANNs were used to obtain the 2 performance parameters for varying twists.

The ANNs were trained for each of these parameters and their predictions can be seen in Figure15. The objective function used was:

$$OFV = 0.48FM_{max} - 0.52\nabla FM - 0.04 \quad (23)$$

The GA was then run and the results shown in Figure 16(a) suggested a twist value of between 15 and 16 degrees. Figure 16(b) shows the FM vs. collective plot for two of the optima, 15.33 degrees and 16 degrees. It can be seen that at these twist values, a high FM is attained and that at the lower thrust, a higher FM is maintained for a compromise in the FM at high thrust values.

3.2 JMRTS Fuselage

The JMRTS fuselage is a generic fuselage designed for investigating the aerodynamics of a rotor/fuselage in forward flight. Here, it is used as a demonstration of the capability of this optimisation procedure to improve the drag characteristics of a simplified fuselage. The conditions of flight are those used to obtain the experimental data i.e. Mach number of 0.175 and Re = 1.1 million[45] . An initial solution of the original geometry was obtained (Figure 17(a)) and the results showed that the front cone area of the fuselage (x = -0.68 to x = -0.4) produced approximately 61% of the total pressure drag, the doghouse area (x = -0.4 to x = -0.2) produced approximately 19% of the pressure drag and the back slant (x=-0.2 to 0.4), approximately 17%. This suggests that the front area of the fuselage could benefit from aerodynamic optimisation.

Therefore, for a first set of comparisons, a modified fuselage was created that reduced the gradient of the 2 regions mentioned above as shown in Figure 17(b). Figure 18 also shows the C_p distribution for some stations along the centreline for both fuselages. The pressure slices amplify the differences between the two shapes.

The total drag (pressure and friction) for the original, parameterised and optimised shapes is shown in Table 3. The overall drag of the original body was very close to the parameterised shape. This suggests that the coefficient of Table 1 can accurately represent the JMRTS shape. Table 3 also shows the reduction of the drag obtained for the front part of the fuselage. As a result of the optimisation, a slight increase of the volume of the body was also obtained. This increase in volume

of the body caused by the change in shape was approximately 0.8% and was combined with a 0.2% decrease in surface area. This shows that significant drag improvements can be made for an almost insignificant change in the total volume of the body.

Also included in Table 3, is the drag of the parameterised fuselage with an actuator disk above it. The actuator disk simulates the effect of a rotor by creating a pressure difference on a single plane inside the flow. The employed actuator disk had a uniform load distribution and produced a C_T value similar to settings of the JAXA experiments[45] . The disk was defined by its radius, centre and thickness as well as the C_T and μ of the rotor. The change in dimensionless pressure is then given by

$$\Delta P = \mu^2 C_T \tag{24}$$

The actuator disk was added here to allow for the stagnation points near the front and rear of the fuelage to be somehow closer to reality since an isolated fuselage computation would have no influence from the rotor. The overall effect of the actuator disk was to increase the magnitude of drag but this resulted in a more realistic flow-field around the fuselage.

4 Conclusions and future work

The optimisation technique described in this work was applied to the optimisation of anhedral and sweep optimisation in forward flight. The twist of the optimised planform was then optimised in hover. A genetic algorithm (GA) was successfully used for the optimisation. It relied on a meta-model based on an Artificial Neural Network (ANN) that was used and trained using a database of CFD computed cases. The ANN was coupled with the GA to predict each load involved in the optimisation function. These loads with an appropriate user-defined weight were combined to obtain the 'fitness' of an individual design. After a number of generations, the offspring tended to have very similar characteristics with very high fitness values.
The anhedral and sweep of the rotor tip was optimised to reduce the overall and vibratory pitching moment of the blade. Increasing the anhedral and reducing the sweep of the UH60-A resulted in a 25% decrease in average pitching moment, a 17% reduction in peak-to-peak pitching moment and a 6% decrease in torque coefficient, with a penalty of a 5% increase in vibratory pitching moment. The new anhedral and sweep values also improved the hover performance which was further improved by reducing the twist very slightly (0.67 degrees).
For the fuselage, the JAXA JMRTS fuselage was parameterised using the ROBIN body parameterisation technique and a preliminary analysis was carried out. It was found that the drag can be reduced quite significantly with very simple changes to the front area. The volume and the surface area were constrained and the method allowed for very efficient computations. The effect of the rotor disk was approximated by an actuator disk model.

The novelty of the proposed method is that the effects on the loads due to specific and small design changes as predicted by a high-fidelity solver, can still be captured with little loss in efficiency and cost thanks to the employed meta-model. The major cost in this procedure is building the database of CFD cases. In the future, the aim is to apply this procedure to forward flight optimisation of blade twist as well and also to extend this procedure to fuselage optimisation. The main limitation with design optimisation of rotors is the computational cost and time which is due to the high-fidelity CFD computations required to build the initial database. Therefore a key part of design optimisation will be the use of fast CFD prediction methods especially for more complex design optimisations and large cases. In the future, methods like the Harmonic Balance approach of[29] will be used for the optimisation and validated with the time marching method. It is also envisaged that fuselage and rotor body interaction will also be studied.

The Optimisation and ANN algorithms are available to interested readers in source code format.

Acknowledgment: C. S. Johnson is supported by an ORSAS Award from the University of Liverpool. The authors would like to acknowledge the use of the JMRTS fuselage and experimental data of JAXA.

References

[1] Celi, R. and Friedmann, P. P., Structural Optimization with Aeroelastic Constraints of Rotor Blades with Straight and Swept Tips, *AIAA Journal*, vol.28, Issue 5, p.928-936, May 1990.

[2] Friedmann, P. P., Helicopter Vibration Reduction Using Structural Optimization with Aeroelastic/Multidisciplinary Constraints - A survey, *Journal of Aircraft*, vol.28, Issue 1, p.8-21, January 1991.

[3] Yuan, K., Friedmann, P. P., Structural Optimization for Vibratory Loads Reduction of Composite Helicopter Rotor Blades with Advanced Geometry Tips, *Journal of the American Helicopter Society*, vol.43, Issue 3, p.246-256, July 1998.

[4] Celi, R., Recent Applications of Design Optimization to Rotorcraft - A survey, *Journal of Aircraft*, vol.36, Issue 1, p.176-189, January-February 1999.

[5] Ganguli, R., Survey of Recent Developments in Rotorcraft Design Optimization, *Journal of Aircraft*, vol.41, Issue 3, p.493-510, May-June 2004.

[6] Walsh, J. L., Performance Optimisation of Helicopter Rotor Blades, *NASA Technical Memorandum*, TM-104054, NASA, April 1991.

[7] Le Pape, A., Beaumier, P., Numerical Optimisation of Helicopter Rotor Aerodynamics Performance in Hover, *Journal of Aerospace Science and Technology*, vol.9, Issue 3, p.191-201, April 2005.

[8] Imiela, M., High-Fidelity Optimization Framework for Helicopter Rotors, *35th European Rotorcraft Forum*, [CD-ROM] Paper 101172, Hamburg, Germany, September 2009.

[9] Glaz, B., Friedmann, P. P. and Liu, L., Surrogate Based Optimization of Helicopter Rotor Blades for Vibration Reduction in Forward Flight, *Structural Multidisciplinary Optimisation*, DOI: 10.1007/s00158-007-0137-z, vol.35, Issue 4, p.341-363, 2008.

[10] Glaz, B., Friedmann, P. P. and Liu, L., Helicopter Vibration Reduction Throughout the Entire Flight Envelope Using Surrogate Based Optimization, *Journal of the American Helicopter Society*, vol.54, p.012007-1-012007-15, January 2009.

[11] Tatossian, C., Nadarajah, S. K. and Castonguay, P., Aerodynamic Shape Optimization of Hovering Rotor Blades using a Non-linear Frequency Domain Approach, AIAA 2008-322, *46th AIAA Aerospace Sciences Meeting and Exhibit*, Reno, Nevada, USA, 7 - 10 January 2008.

[12] Allen, C. B., Rendall, T. C. S. and Morris, A. M., CFD-Based Twist Optimization of Hovering Rotors, AIAA 2010-676 *48th AIAA Aerospace Sciences Meeting Including the New Horizons Forum and Aerospace Exposition*, Orlando, Florida, USA, 4 - 7 January 2010.

[13] Chae, S., Yee, K., Jeong, S., Obayashi, S., Helicopter Rotor Shape Optimization for the Improvement of Aeroacoustic Performance in Hover, *Journal of Aircraft*, DOI: 10.2514/1.C000283, vol.47, Issue 5, p.1770-1783, September-October 2010.

[14] Caradonna, F. X. and Tung, C., Experimental and Analytical Studies of a Model Helicopter Rotor in Hover, *NASA Technical Memorandum*, NASA-TM-81232, NASA, September 1981.

[15] Caradonna, F. X., The Application of CFD to Rotary Wing Problems, *NASA Technical Memorandum*, NASA-TM-10280, NASA, March 1992.

[16] Keys, C., Tarzanin and F., McHugh, F., Effect of twist on helicopter performance and vibratory loads, *13th European Rotorcraft Forum*, paper 2-7, Arles, France, September 8-11, 1987.

[17] Martin, P. B., Leishman, J.G., Trailing Vortex Measurements in the Wake of a Hovering Rotor Blade with Various Tip Shapes, *58th Annual Forum of the American Helicopter Society, Montreal, Canada*, [CD-ROM], June 11-13, 2002.

[18] Vanderplaats, G. N., CONMIN - A FORTRAN Program for Constrained Function Minimisation, User's Manual, *NASA Technical Memorandum*, TM X-62,282, NASA, August 1973.

[19] Schwabacher, M., Ellman, T. and Hirsh, H., Learning to Set Up Numerical Optimisations of Engineering Designs, *Artificial Intelligence for Engineering Design, Analysis and Manufacturing Journal*, vol.12, Issue 2, p.173-192, April 1998.

[20] Chen, C. and Lee, H., An Efficient Gradient Forecasting Search Method Utilising the Discrete Difference Equation Prediction Model, *Applied Intelligence Journal* vol.16, Issue 2, p.43-58, 2002.

[21] Mohammadi, B. and Pironneau, O., Shape Optimisation in Fluid Mechanics, *Annual Reviews of Fluid Mechanics*, vol.36, p.255-79, 2004.

[22] Watanabe, T., Matsushima, K. and Nakahashi, K., Aerodynamic Shape Optimization of a Near-Sonic Passenger Plane using Computational Fluid Dynamics, *Proceedings of IMechE*, Part G: *Journal of Aerospace Engineering*, DOI: 10.1243/09544100JAERO349, vol.222, Issue 7, p.1025-1035, 2008.

[23] Zhao, H., Wang, S., Han, W. and Feng, G., Aerodynamic Design by Jointly Applying S2 Flow Surface Calculations and Modern Optimization Methods on Multistage Axial Turbines, *Frontiers of Energy Power Engineering, China*, vol.2, Issue 1, p.93-98, 2008.

[24] Samad, A., Kim, K. Y., Shape Optimization of an Axial Compressor Blade by Multiobjective Genetic Algorithm, *Proceedings of IMechE*, Part A: *Journal of Power and Energy*, DOI: 10.1243/09576509JPE596, vol.222, Issue 6, p.599-611, June 2008.

[25] Mengistu, T. and Ghaly, W., Aerodynamic Optimization of Turbomachinery Blades using Evolutionary Methods and ANN-based Surrogate Models, *Optimisation Engineering Journal*, DOI: 10.1007/s11081-007-9031-1, vol.9, Issue 3, p.239-255, 2007.

[26] Le Pape, A., Numerical aerodynamic optimization of helicopter rotors: multi-objective optimization in hover and forward flight conditions, *31st European Rotorcraft Forum*, [CD-ROM] Paper 98, Florence, Italy, Sept 13-15 2005.

[27] Hirsh, R., GADO: A Genetic Algorithm for Continuous Design Optimization, *PhD thesis, State University of New Jersey*, New Jersey, 1998.

[28] Steijl, R., Barakos, G. and Badcock, K., A framework for CFD Analysis of Helicopter Rotors in Hover and Forward Flight, *International Journal of Numerical Methods in Fluids*, DOI: 10.1002/fld.1086, vol.51, p.819-847, Jan 2006.

[29] Woodgate, M., Barakos, G.N., Implicit CFD Methods for Fast Analysis of Rotor Flows, *36th European Rotorcraft Forum*, ERF pp.1, Paris, France, Sept, 2009.

[30] Srinivasan, G. R., A Free-Wake Euler and Navier-Stokes CFD Method and its Application to Helicopter Rotors Including Dynamic Stall, *JAI Associates, Inc. Science and Engineering Consultants* AD-A278 000, Technical Report 93-01, April 1994.

[31] Wilcox, D. C., *Turbulence Modelling for CFD*, 2nd edition, ISBN-10: 1928729088, DCW Industries, USA, 2006.

[32] Steijl, R., Barakos, G. N. and Badcock, K. J., Computational Study of the Advancing Side Lift-Phase Problem, *Journal of Aircraft*, DOI: 10.2514/1.22044, vol.45, no.1, Jan-Feb 2008.

[33] Datta, A., and Chopra, I., Validation of Structural and Aerodynamic Modeling Using UH-60A Flight Test Data, *American Helicopter Society 59th Annual Forum*, AHS International, Alexandria, VA, May 2003.

[34] Leishman J. G., *Principles of Helicopter Aerodynamics*, 2nd edition, ISBN-10: 0521858607, Cambridge Aerospace Series, New York, USA, 2006.

[35] ANSYS Inc., ICEM-CFD Hexa Mesh Generation Software, *http://www.ansys.com/products/icemcfd.asp*.

[36] Samarasinghe, S. Neural Networks for Applied Sciences and Engineering - From Fundamentals to Complex Pattern Recognition, *Auerbach Publications*, ISBN-10: 0-8493-3375-X, New York, USA, 2006.

[37] Spentzos, A., Barakos, G., Badcock, K. and Richards, B., Modelling 3-Dimensional Dynamic Stall of Helicopter Blades using Computational Fluid Dynamics and Neural Networks, *Proceedings of IMechE* Part G: *Journal of Aerospace Engineering*, DOI: 10.1243/09544100JAERO101, vol. 220, Issue 6, p.605-618, 2005.

[38] Régnier, J., Sareni, B. and Roboam, X., System Optimization by Multi-Objective Genetic Algorithms and Analysis of the Coupling between Variables, Constraints and Objectives", *The International Journal for Computation and Mathematics in Electrical and Electronic Engineering*, DOI 10.1108/03321640510598157, vol. 24, Issue 3, p.805-820, 2005.

[39] Ahmed, M. Y. M. and Qin, N., Meta-models for Aerothermodynamic Design Optimization of Hypersonic Spiked Blunt Bodies, *University of Sheffield, UK, Jan 2010*.

[40] Lophaven, S. N., Nielsen, H. B. and Sondergaard, J., DACE, A MATLAB Kriging Toolbox Version 2.0 August 1, 2002, *IMM Informatics and Mathematical Modelling*, Technical Report IMM-TR-2002-12, Technical University of Denmark DK-2800 Kgs. Lyngby Denmark, August 2002.

[41] Johnson, C. S. and Barakos, G. N., Development of a Framework for Optimising Aspects of Rotor Blades, *Paper 377 [CDROM] American Helicopter Society Forum*, Phoenix, Arizona, USA, May 2010.

[42] Johnson, C. S. and G. Barakos, G. N., A Framework for Optimising Aspects of Rotor Blades, *Aeronautical Journal, Royal Aeronautical Society*, Accepted Nov 2010.

[43] Johnson, C. S. and Barakos, G. N., Optimising Aspects of Rotor Blades in Forward Flight, *49th AIAA Aerospace Sciences Meeting including the New Horizons Forum and Aerospace Exposition*, Orlando, Florida, USA, 4-7th Jan 2011.

[44] Berry, J. D., Althoff S. L., Computing Induced Velocity Perturbations Due to a Helicopter Fuselage in a Freestream, *NASA Technical Memorandum 4113*, 1989.

[45] Hideaki Sugawara, Yasutada Tanabe, Shigeru Saito, A Numerical Study of Rotor/Fuselage Interaction Based on the JMRTS Database, Japan Aerospace Exploration Agency, Ryoyu Systems Co., Ltd., Heli Japan 2010, Saitama, Japan, Nov 2010.

Parameter	C1	C2	C3	C4	C5	C6	C7	C8
x = 0.015 to 0.06, Δx = 0.02								
H	0.300	-62.60	-0.150	0.700	4.000	-0.210	1.500	1.001
W	0.965	-0.950	-0.400	0.400	1.800	0.035	0.420	1.800
Y_o	0.000	0.000	0.000	0.000	0.000	0.000	0.000	0.000
Z_o	0.050	-0.050	0.000	1.000	1.000	0.000	0.200	1.001
N_{up}	2.000	0.080	0.000	0.400	1.000	0.000	0.000	1.000
N_{lw}	2.000	-0.064	0.000	0.400	1.000	0.000	0.000	1.000
x = 0.06 to 0.24, Δx = 0.05								
H	0.460	-0.770	-0.500	0.700	2.500	0.000	0.000	1.000
W	0.960	-1.000	-0.400	0.400	1.800	0.055	0.410	1.800
Y_o	0.000	0.000	0.000	0.000	0.000	0.000	0.000	0.000
Z_o	0.006	0.020	-0.240	1.000	1.000	0.000	0.000	1.000
N_{up}	2.000	0.080	0.000	0.400	1.000	0.000	0.000	1.000
N_{lw}	2.100	-0.230	0.000	0.400	1.000	0.000	0.000	1.000
x = 0.24 to 0.30, Δx = 0.05								
H	0.345	2.000	0.000	0.700	3.500	0.000	0.000	1.000
W	0.950	-1.000	-0.400	0.400	1.800	0.055	0.410	1.800
Y_o	0.000	0.000	0.000	0.000	0.000	0.000	0.000	0.000
Z_o	0.009	3.500	-0.250	1.000	2.000	0.000	0.000	1.000
N_{up}	2.000	0.080	0.000	0.400	1.000	0.000	0.000	1.000
N_{lw}	2.000	-0.064	0.000	0.400	1.000	0.000	0.000	1.000
x = 0.30 to 0.44, Δx = 0.05								
H	0.400	1.645	-0.220	0.920	1.500	0.000	0.000	1.000
W	0.446	-1.000	-0.460	0.500	4.000	0.000	0.000	1.000
Y_o	0.000	0.000	0.000	0.000	0.000	0.000	0.000	1.000
Z_o	-0.005	0.850	-0.220	0.920	1.500	0.005	0.855	1.001
N_{up}	2.200	3.403	-0.280	0.200	2.000	0.000	0.000	1.000
N_{lw}	1.500	0.690	0.000	0.400	1.000	0.000	0.000	1.000
x = 0.44 to 0.58, Δx = 0.06								
H	0.620	-3.950	-0.560	0.920	2.500	0.000	0.000	1.000
W	0.450	-1.000	-0.460	0.500	4.000	0.000	0.000	1.000
Y_o	0.000	0.000	0.000	0.000	0.000	0.000	0.000	1.000
Z_o	0.099	-2.800	-0.560	1.000	2.500	0.000	0.000	1.000
N_{up}	3.866	0.800	-0.280	0.200	2.000	0.000	0.000	1.000
N_{lw}	1.550	0.650	0.000	0.400	1.000	0.000	0.000	1.000
x = 0.58 to 0.88, Δx = 0.05								
H	0.620	-0.070	-0.580	1.000	2.000	0.000	0.000	0.000
W	0.448	0.000	0.000	0.000	0.000	0.000	0.000	0.000
Y_o	0.000	0.000	0.000	0.000	0.000	0.000	0.000	0.000
Z_o	0.099	-0.005	-0.580	1.000	2.000	0.000	0.000	0.000
N_{up}	5.600	0.000	0.000	1.000	0.000	0.000	0.000	0.000
N_{lw}	1.400	1.000	0.000	1.000	0.000	0.000	0.000	0.000
x = 0.88 to 1.16, Δx = 0.05								

Continued on Next Page...

Table 1 – Continued

Parameter	C1	C2	C3	C4	C5	C6	C7	C8
H	0.612	-1.000	-0.880	1.100	1.500	0.000	0.000	1.000
W	0.450	-0.525	-0.800	1.100	2.500	0.000	0.000	1.000
Y_o	0.000	-0.000	-0.000	0.000	0.000	0.000	0.000	0.000
Z_o	0.100	-0.400	-0.880	1.000	1.500	0.032	6.500	0.500
N_{up}	5.750	-10.00	-0.800	1.100	1.000	0.000	0.000	0.000
N_{lw}	2.680	-0.530	-0.600	0.500	1.000	0.000	0.000	0.000
x = 1.16 to 1.26, Δx = 0.05								
H	1.000	-1.300	-0.900	1.100	1.000	0.312	0.360	0.500
W	0.450	-0.525	-0.800	1.100	2.500	0.000	0.000	1.000
Y_o	0.000	-0.000	-0.000	0.000	0.000	0.000	0.000	0.000
Z_o	1.000	0.290	-1.270	0.800	1.000	-0.094	0.120	0.330
N_{up}	3.750	-2.805	-0.665	1.100	1.000	0.000	0.000	0.000
N_{lw}	2.750	-0.580	-0.600	0.500	1.000	0.000	0.000	0.000
x = 1.26 to 1.51, Δx = 0.05								
H	0.445	-1.400	-1.120	0.800	2.500	0.000	0.000	1.000
W	0.410	-3.400	-1.000	1.100	3.500	0.000	0.000	1.000
Y_o	0.000	-0.000	-0.000	0.000	0.000	0.000	0.000	0.000
Z_o	0.027	0.012	-1.280	1.000	1.000	0.000	0.000	0.000
N_{up}	2.600	-0.804	-0.800	1.100	1.000	0.000	0.000	0.000
N_{lw}	2.230	-0.550	-0.800	1.000	1.000	0.000	0.000	0.000
x = 1.51 to 1.548, Δx = 0.02								
H	0.175	-2.400	-1.530	0.800	1.000	0.000	0.000	1.000
W	0.142	-2.500	-1.530	1.100	1.000	0.000	0.000	1.000
Y_o	0.000	-0.000	-0.000	0.000	0.000	0.000	0.000	0.000
Z_o	0.027	0.040	-1.280	1.000	1.000	0.000	0.000	0.000
N_{up}	4.900	-4.404	-0.800	1.100	1.000	0.000	0.000	0.000
N_{lw}	2.300	-0.600	-0.800	1.000	1.000	0.000	0.000	0.000

Table 1: *Parameters for the JMRTS Fuselage by JAXA.*

Sweep(deg)	Anhedral(deg)	$\overline{C_m^{pitch}}$	$\Delta C_m{}^{\text{pitch}}$	$\Delta C_m{}^{\text{vib-pitch}}$	C_Q	OFV	Remark
20.0	0.00	1.0000	1.0000	1.0000	1.000	0.000	original
20.0	15.00	0.7485	0.8145	1.1245	0.906	0.183	best in initial popn
17.1	11.00	0.7594	0.8239	1.0525	0.933	0.209	best new design by GA

Table 2: *Comparison of optimised and original UH60-A rotor blade in terms of pitching moment performance.*

Description	Drag coefficient
Original full body	0.02110
Parameterised full body	0.02108
Parameterised front fuselage	0.007575
Optimised front fuselage	0.005979

Table 3: *Comparison of drag for the original, parameterised and optimised JMRTS fuselages.*

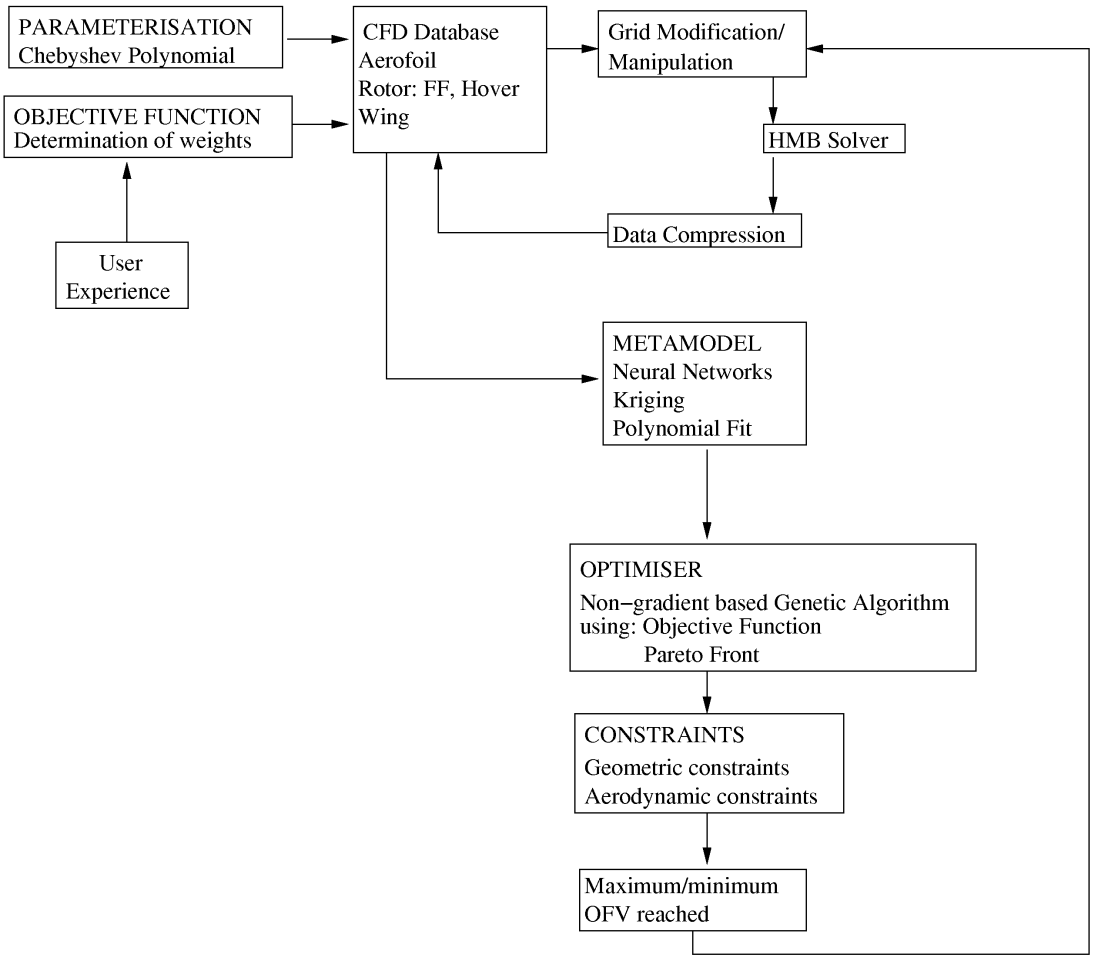

Figure 1: *Map of the processes involved in the optimisation of rotor blades.*

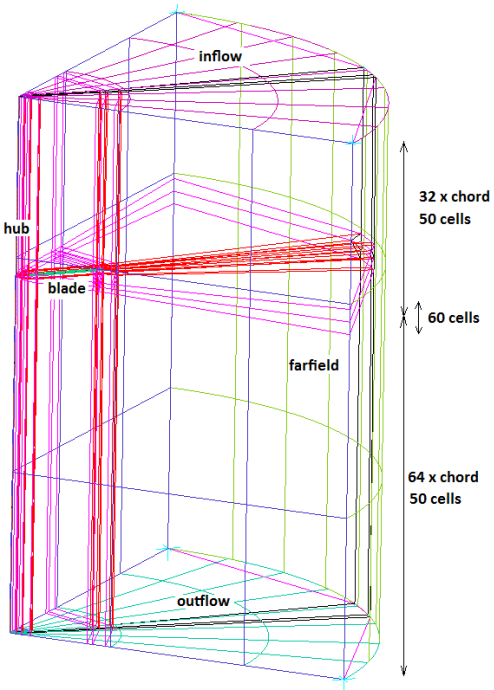

Figure 2: *Topology, domain boundaries and cells.*

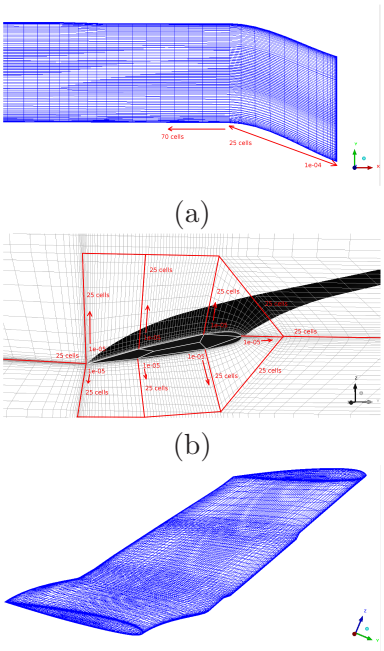

Figure 3: *UH60-A blade mesh (a) top view (b) mesh perpendicular to tip (c) full length view, high mesh density at the tip and the change of blade sections.*

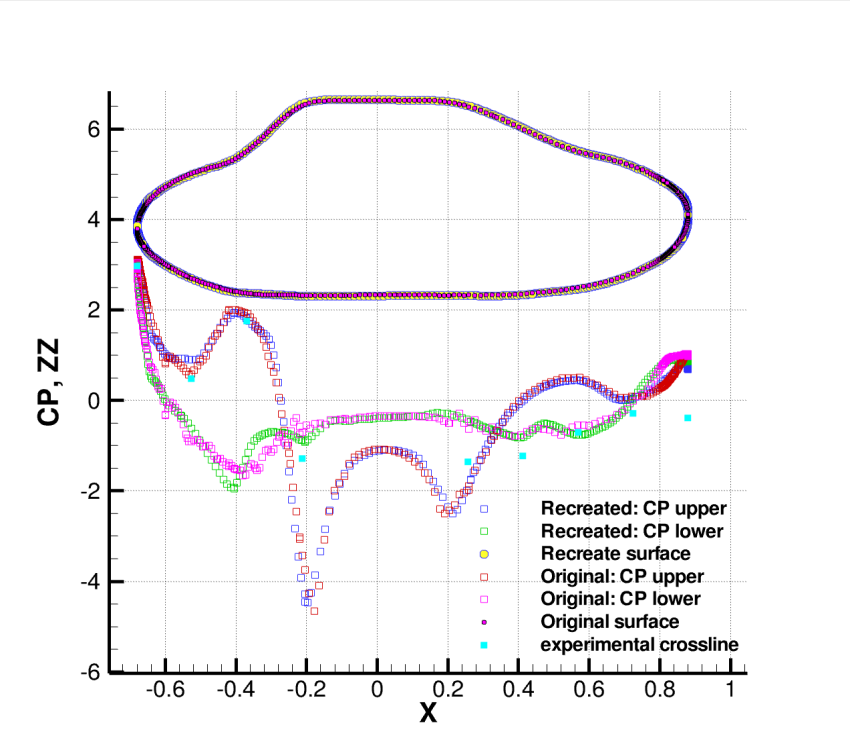

Figure 4: *C_p distribution of the original fuselage (green), the parameterised fuselage (red) and the experimental data (blue).*

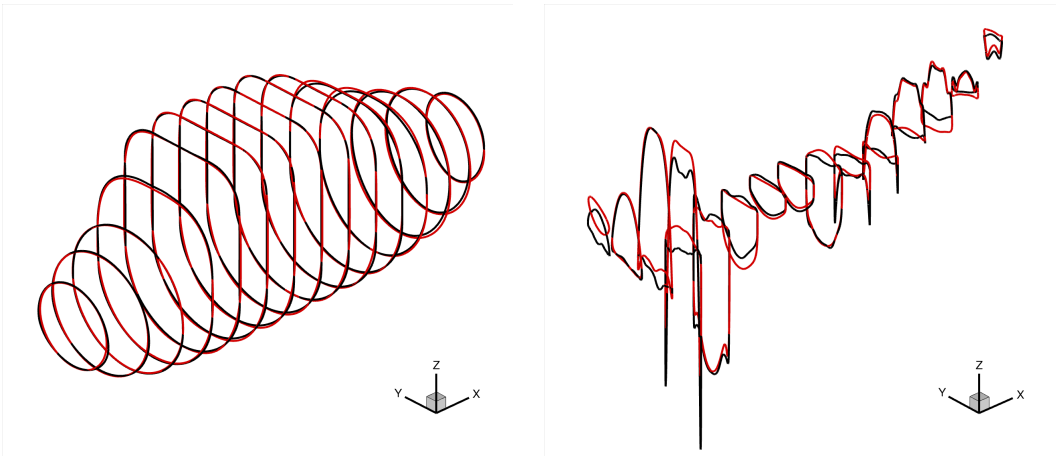

Figure 5: *Pressure distribution comparison between the original and the parameterised shape.*

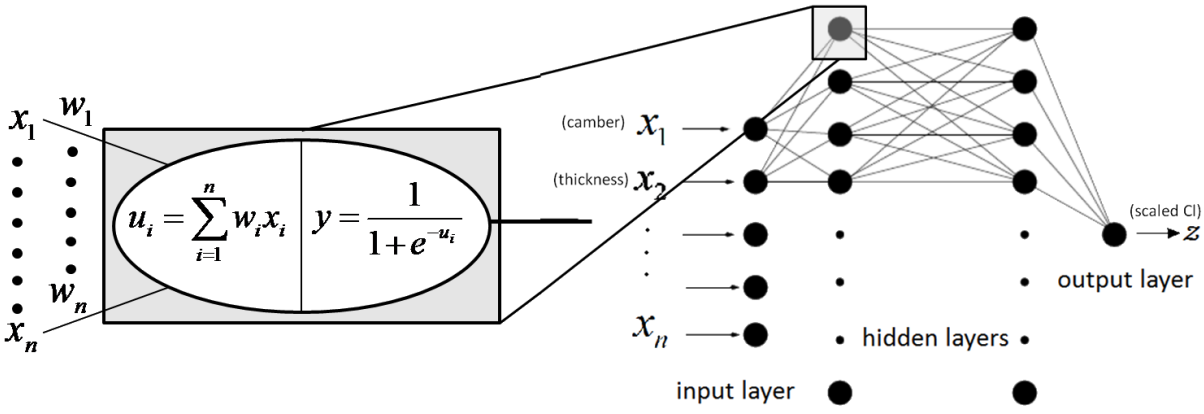

Figure 6: *An example of a neural network trained to receive inputs x_i, to obtain an output z (Spentzos, Barakos, Badcock and Richards, 2005).*

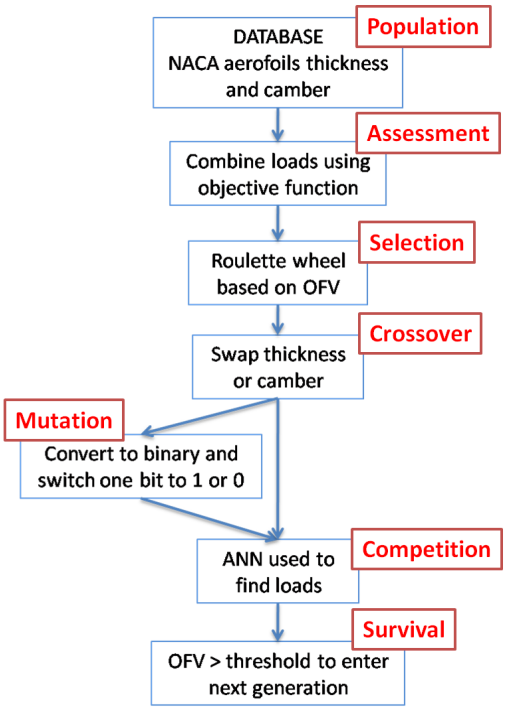

Figure 7: *Outline of the genetic algorithm employed for an aerofoil selection case and the analogy with genetics.*

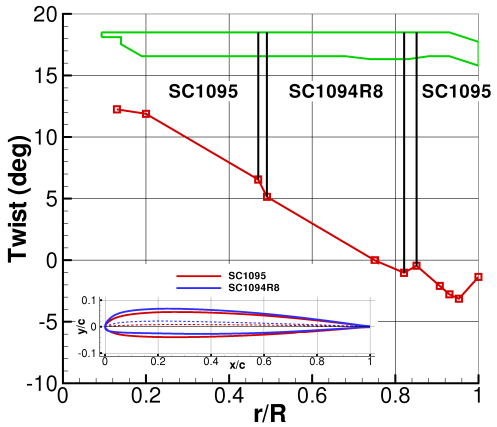

Figure 8: *UH60-A rotor blade twist and aerofoil distribution.*

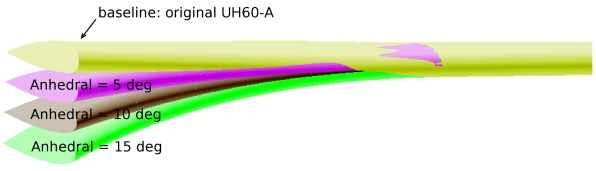

Figure 9: *Anhedral variation as smooth arc.*

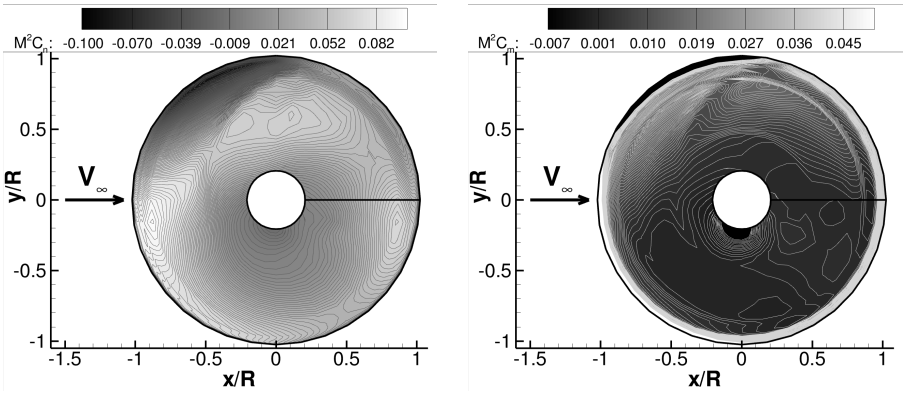

original: sweep 20, anhedral 0

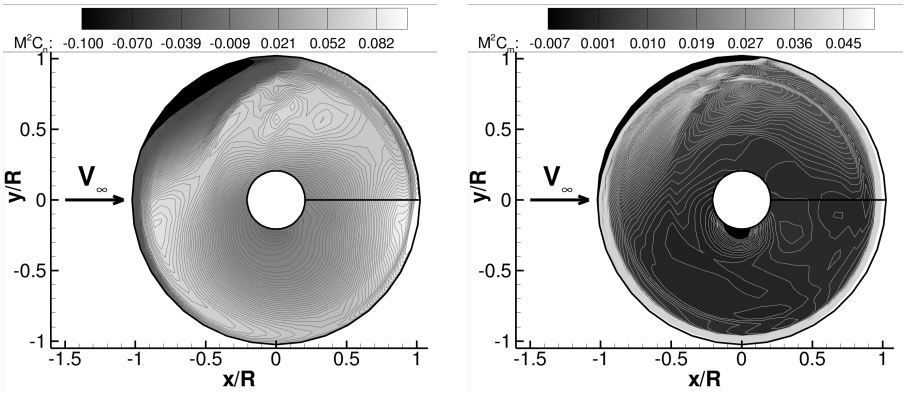

sweep 20, anhedral 15

Figure 10: *M^2C_n and M^2C_m plots for the UH60-A with different anhedral.*

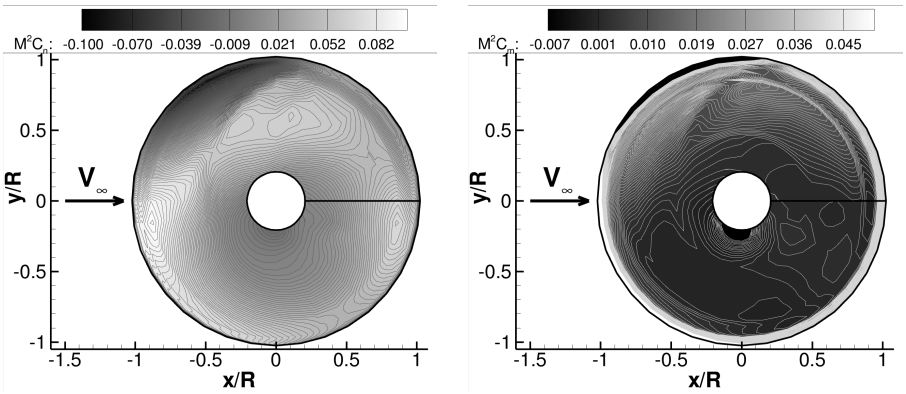

original: sweep 20, anhedral 0

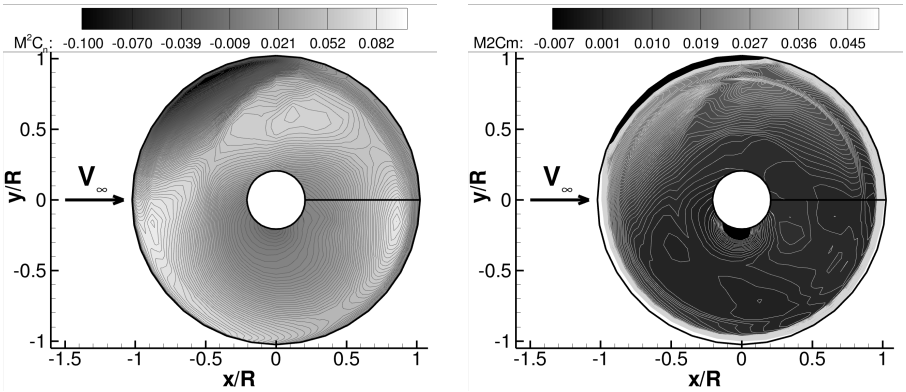

sweep 40, anhedral 0

Figure 11: *M^2C_n and M^2C_m plots for the UH60-A with different sweep.*

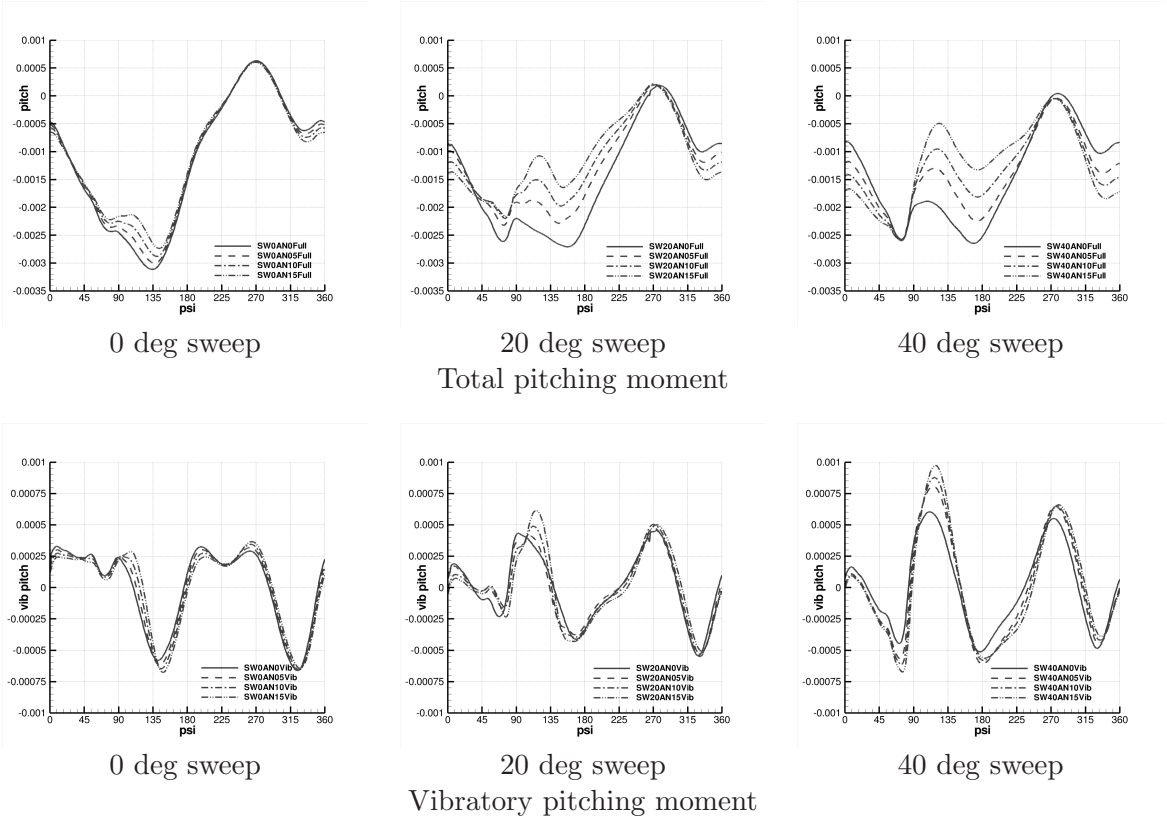

0 deg sweep | 20 deg sweep | 40 deg sweep

Total pitching moment

0 deg sweep | 20 deg sweep | 40 deg sweep

Vibratory pitching moment

Figure 12: *Total and vibratory pitching moments for a single blade over a revolution of the rotor in forward flight. The original rotor has 20 degrees sweep and 0 degrees anhedral.*

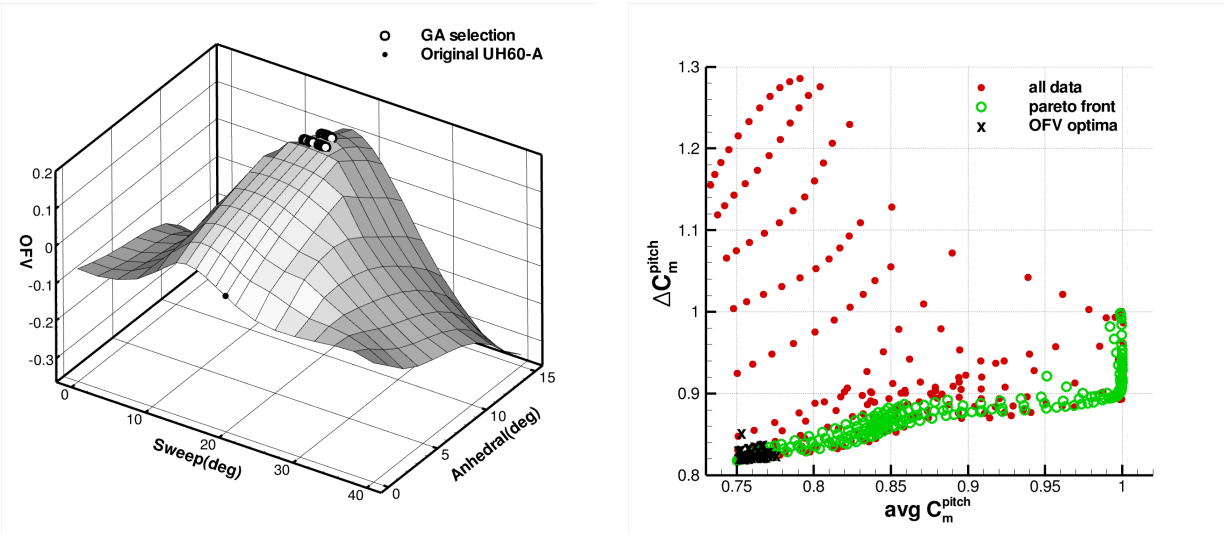

(a) (b)

Figure 13: *(a) Genetic algorithm results, (b) Comparison between Pareto front optimisation and objective function selection.*

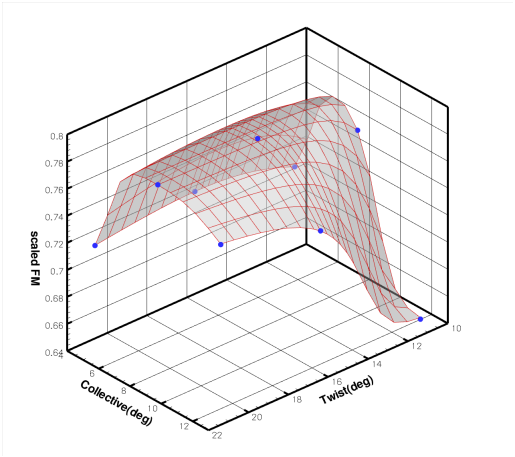

Figure 14: *FM vs. collective and twist settings predictions for the ANN as well as the CFD training data.*

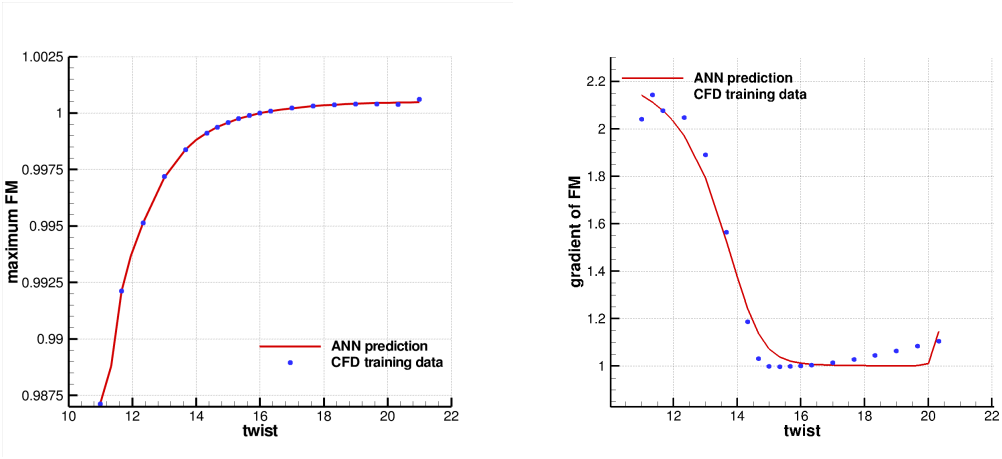

(a) (b)

Figure 15: *ANN predictions for (a) maximum FM and (b) gradient of FM.*

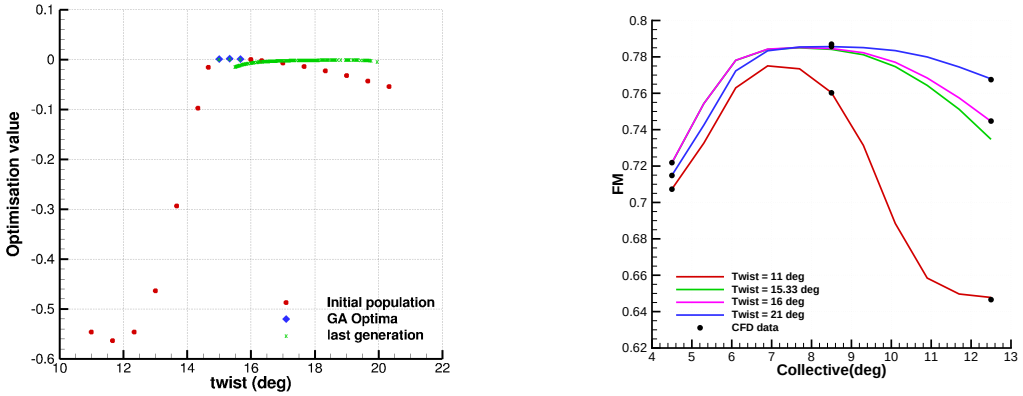

(a) (b)

Figure 16: *(a) GA optimum and (b) FM vs. Collective setting for training values and optimum values of twist.*

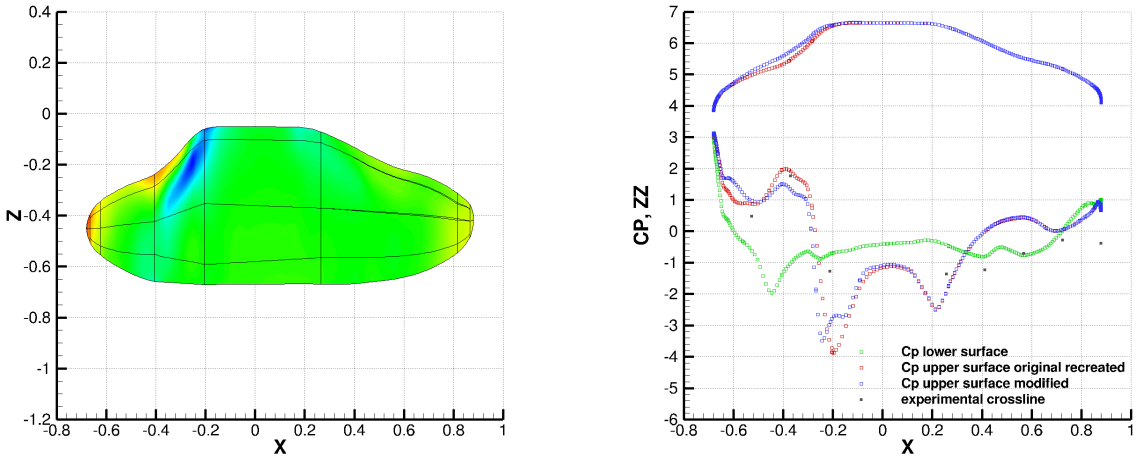

Figure 17: *(a) Parameterised JMRTS fuselage showing x coordinate definitions, (b) C_p distribution along the centreline for the parameterised and the modified JAXA bodies.*

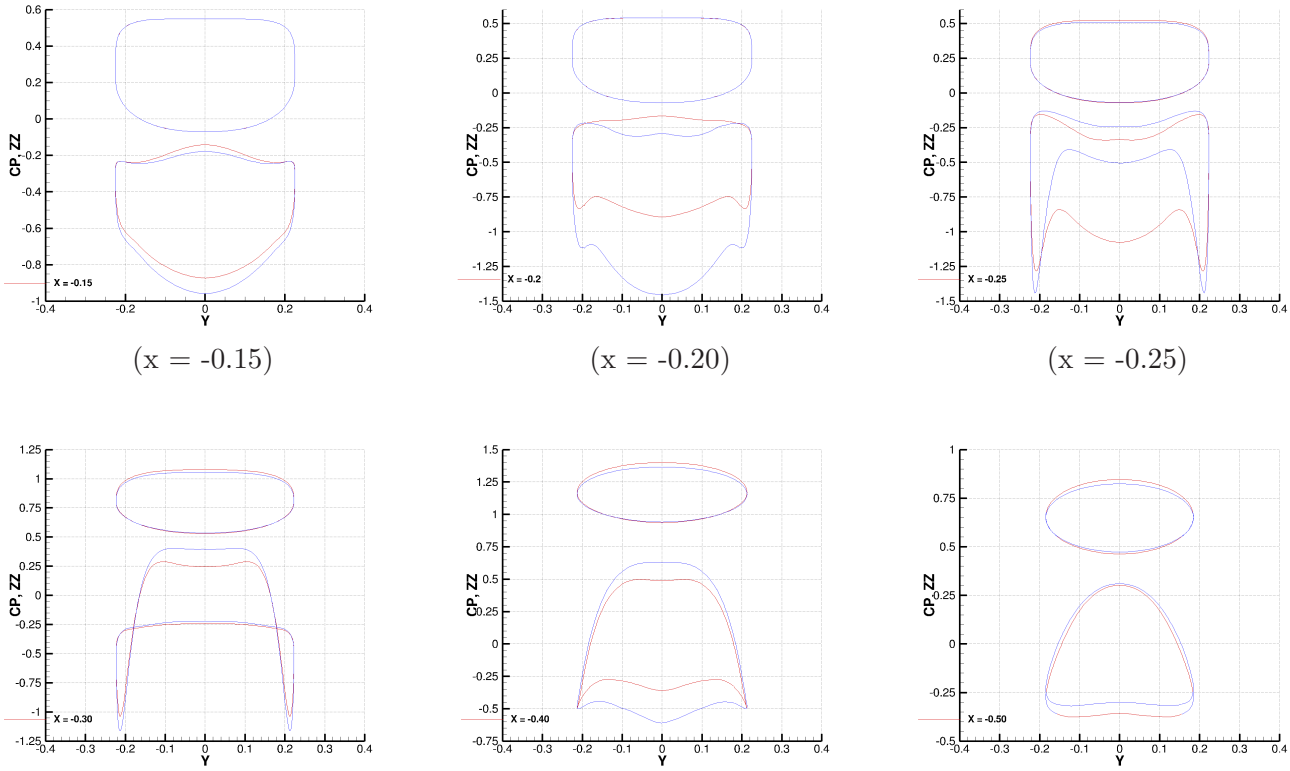

(x = -0.15) (x = -0.20) (x = -0.25)

(x = -0.30) (x = -0.40) (x = -0.50)

Figure 18: *C_p distribution differences along the fuselage of the original parameterised fuselage and the modified one (red is modified and blue is parameterised original).*